Modeling Oscillator Injection Locking Using the Phase Domain Response

Dustin Dunwell, *Student Member, IEEE*, and Anthony Chan Carusone, *Senior Member, IEEE*

***Abstract*—This paper presents a simulation-based model for the behavior of injection-locked oscillators (ILOs) that can be applied to any oscillator topology under any strength of injected signal. By using the phase domain response (PDR) of an oscillator, the proposed model is shown to accurately predict the behavior of ILOs with asymmetric lock ranges or those using injection into multiple locations. It can also model subharmonic injection locking behavior. The model is validated through comparison with SPICE simulations as well as measured results of a multiplying ILO fabricated in 65-nm CMOS.**

***Index Terms*—Frequency multiplication, impulse sensitivity function (ISF), injection locking, jitter tracking, locking range, locking time, phase-domain modeling.**

I. Introduction

INJECTION-LOCKED oscillators (ILOs) are becoming increasingly common as frequency dividers [1], multipliers [2], or as alternatives to phase-locked loops (PLLs) [3]. This is due in large part to their small power and area requirements as well as their ability to operate at high speeds [1] and to quickly transition between operating states [4].

Due to their potential for ubiquitous use, a great deal of attention has recently been paid to developing a comprehensive model of the injection-locking behavior of oscillators. Despite this, an ILO model that is accurate, intuitive and applicable for all types of oscillators under any strength of injection signal has yet to be developed. This paper analyzes the strengths and weaknesses of both the frequency domain model, first proposed in [5], and the more recently proposed phase domain model [6], which is based on the impulse sensitivity function (ISF) of an oscillator [7]. It then proposes a new model using the phase domain response (PDR) of an ILO, which can easily be extracted from and applied to any oscillator under any type of injected signal. The utility of this new model is then demonstrated by using it to develop an ILO with a wide lock range.

II. The Frequency Domain Model

An early model used to describe injection locking phenomena observed in LC oscillators was developed in [5]. In this model the phase difference between the injected and free running oscillator signals, $\Delta\phi(t)$, was derived as

$$\frac{d\Delta\phi(t)}{dt} = \Delta\omega - \frac{I_{inj}}{I_{osc}}\frac{\omega_0}{2Q} sin\left(\Delta\phi(t)\right) \tag{1}$$

where ω_0 is the free running oscillator frequency, $\Delta\omega$ is the difference between ω_0 and the injected signal frequency, Q is the quality factor of the tank, I_{inj} is the injected signal strength, and the strength of the free running oscillations is I_{osc}.

When the injection locked oscillator has settled to a steady state then

$$\frac{d\Delta\phi(t)}{dt} = 0 \tag{2}$$

and (1) can be simplified to

$$\Delta\omega = \frac{I_{inj}}{I_{osc}}\frac{\omega_0}{2Q} sin(\Delta\phi_0) \tag{3}$$

From this, the lock range, $\Delta\omega_{max}$, of the injection locked oscillator can be found to be

$$\Delta\omega_{max} = \frac{I_{inj}}{I_{osc}}\frac{\omega_0}{2Q} \tag{4}$$

Although this original analysis proved accurate for the case studied in [5], it relied on the following assumptions:

- The injected input and oscillator output are both sinusoidal.
- The oscillator uses an LC tank (since Q is required).
- The strength of the injected signal is much smaller than that of the free running oscillator.

As a result, many later publications have since expanded on this model to make it suitable for large injection strengths [8], [9], ring oscillators [10] and different injected signals such as narrow pulses [8]. These and other works have advanced the frequency domain modeling of ILOs to be able to accurately reflect measured results of their lock range, transient phase step response, jitter tracking bandwidth, and phase noise [11].

Unfortunately, the frequency domain model's accuracy comes at the cost of a loss of generality or increased complexity. While attempts have been made to generalize the frequency domain model [12] to make it applicable in all situations, the results remain complex and difficult to apply during oscillator design. Without a straightforward and intuitive way to determine the effective Q factor, injected signal strength I_{inj}, free-running oscillator strength I_{osc} and whether the ratio I_{inj}/I_{osc} is considered "large," it is extremely difficult for the

Manuscript received September 17, 2012; revised January 15, 2013; accepted February 18, 2013. Date of publication April 11, 2013; date of current version October 24, 2013. This paper was recommended by Associate Editor H. Luong.

The authors are with the Edward S. Rogers Sr. Department of Electrical and Computer Engineering, University of Toronto, Toronto, ON M5S 3G4, Canada (e-mail: dustin.dunwell@mail.utoronto.ca; tcc@eecg.utoronto.ca).

Color versions of one or more of the figures in this paper are available online at http://ieeexplore.ieee.org.

Digital Object Identifier 10.1109/TCSI.2013.2252654

1549-8328 © 2013 IEEE

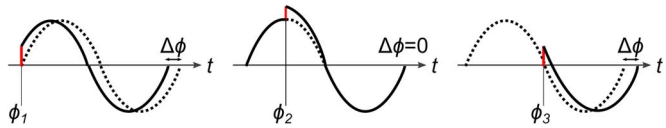

Fig. 1. Impulses applied to an oscillator have varying impacts on the output depending on the relative phase at which they are applied.

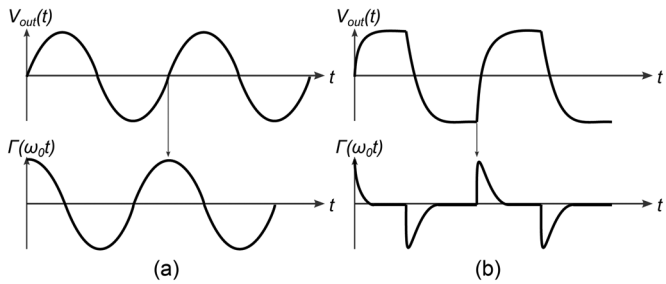

Fig. 2. Example impulse sensitivity functions for oscillators with (a) sinusoidal and (b) square wave outputs.

circuit designer to make use of this model when designing an ILO.

III. The Impulse Sensitivity Function

The ISF was developed in [7] to describe phase noise in oscillators by observing that when small noise current impulses are applied to an oscillator, their impact on the output phase of the oscillator depends on the relative phase at which they are applied. Fig. 1 illustrates this concept, showing that for current impulses applied at phases ϕ_1, ϕ_2 and ϕ_3 the resulting output phase change $\Delta\phi$ is negative, zero or positive, respectively.

It is therefore possible to determine the sensitivity of an oscillator's output phase for all possible applied impulse phases. Typical examples of the resulting impulse sensitivity function, denoted by Γ, are shown in Fig. 2. Note that different injection techniques can produce different Γ functions for a single ILO. Hence, in common practice, simulations of the oscillator in the presence of very small impulsive injections are used to obtain Γ.

The ISF has then traditionally been used to analyze oscillator phase noise and is shown in [7] to have advantages over the Leeson model [13] in its ability to predict $1/f^2$ and $1/f^3$ noise as well as the influence of cyclostationary noise sources. It also offers circuit designers insight into how the shape of the oscillator's output waveform can affect the phase noise performance.

A. ISF-Based ILO Modeling

Although well suited to modeling phase noise, the ISF model cannot be directly applied to model the injection locking behavior of an oscillator [14]. Unlike the noise sources for which the ISF model was developed, the injecting waveforms in ILOs are deterministic. They therefore cause the ISF to change significantly, especially under strong injection. For example, straightforward application of the ISF model cannot account for locking an oscillator to a frequency other than its free-running frequency

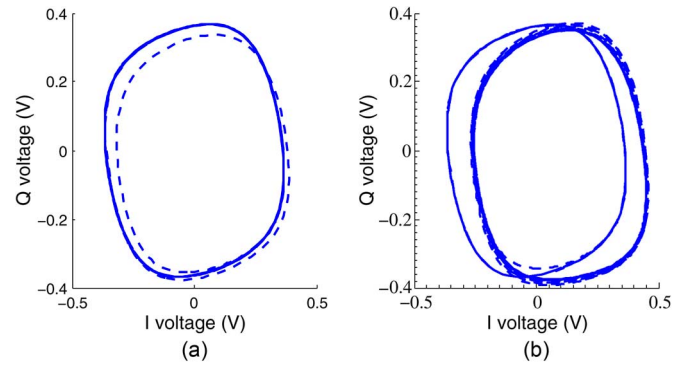

Fig. 3. Simulations of the I and Q states of a four-stage VCO show that (a) an injected impulse causes a perturbation (dotted line) from the steady state (solid line). Repeated impulses (b) can lock the VCO to a different frequency but this requires a new ISF to model the oscillator's new trajectory through state-space.

[14]. This is because, according to the ISF model, the phase at the output of an oscillator can be calculated as

$$\phi(t) = \int_0^t \Gamma(\tau) b(\tau) d\tau \tag{5}$$

where τ is the time of injection and $b(\tau)$ is an injected signal with a period close, but not equal to that of the free-running oscillator, ω_0.

Since $\Gamma(\tau)$ has the same frequency as ω_0, this means that the frequencies of $b(\tau)$ and $\Gamma(\tau)$ will not be equal and that the integral of their product in (5) will contain no dc component. This contradicts the known result for an oscillator that is injection locked to $\omega_{lock} \neq \omega_0$. In this case the output phase of the ILO should increase linearly with time relative to the phase of the free-running oscillator, which should be represented by a dc component in the solution to the integral in (5).

This idea can be represented graphically by examining the I and Q state variables of a four-stage ring oscillator. Simulation results of such an oscillator, reported in Fig. 3(a), show that the injection of an impulse causes a temporary deviation (dotted line) from the steady-state oscillator's trajectory through state-space (solid line), where the magnitude of this deviation is related to the ISF of the oscillator and the strength of the injected impulse. Conventional wisdom dictates that, in order for the ISF to be successfully applied to any future impulses, the transient response of the oscillator must first settle back to its steady-state trajectory. This implies that the oscillator's frequency must remain unchanged and that the ISF is therefore unsuitable for use in the presence of a series of injected impulses designed to lock the ILO to a frequency other than ω_0, since this would result in shifts in the I and Q states as shown in Fig. 3(b) and thereby continuously require new ISFs.

Despite these difficulties, ISF analysis has been successfully adapted to accommodate injection locking. For example, in [6] it is assumed that with each injected impulse, the ILO's Γ function undergoes equivalent changes in phase and any future injected impulses will be applied to the new, phase-shifted ISF as shown in Fig. 4. Although this technique accounts for transient phase changes in the ISF, the model still fails to account

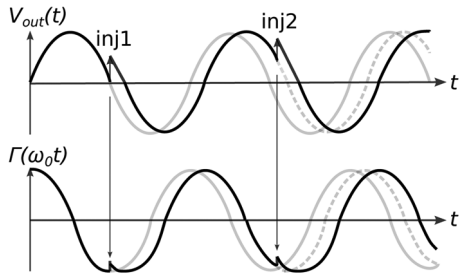

Fig. 4. Injected impulses result in step changes in the oscillator output, which must be accounted for by changing the ISF in order to model injection locking.

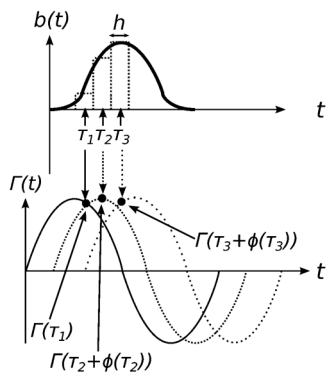

Fig. 5. Dividing an injected signal into impulses that act immediately on the ILO output phase also shift the corresponding $\Gamma(t)$ function, allowing for injection locking to be accurately modeled by the ISF.

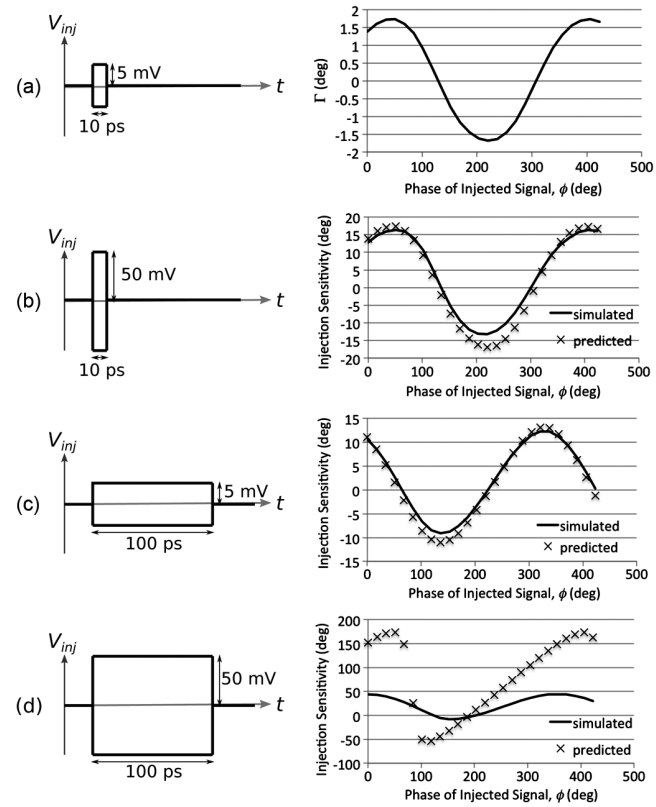

Fig. 6. Simulating an ILO's response to an injected impulse (a) determines the ISF of the oscillator. This ISF can then be used to predict the ILO's sensitivity to pulses with (b) larger amplitudes or (c) wider pulse widths but fails to accurately predict large, wide pulses (d).

for changes in the amplitude or shape of the ISF that inevitably arise when the oscillator's trajectory through state space deviates significantly from its free-running trajectory, as can result from strong injection. Moreover, the analysis is complex and difficult to generalize. As a result, its application commonly relies on simulations to obtain the ISF.

The challenge of modeling oscillators under strong injection is best illustrated by way of example. In Fig. 5 an injected signal is divided into impulses of area $b(\tau)h$. The first impulse produces a shift in oscillator output phase, ϕ, obtained by multiplying the pulse area $b(\tau_1)h$ by $\Gamma(\tau_1)$. In [6], this same phase shift is applied to the ISF so that the second impulse is multiplied by $\Gamma(\tau_2 + \phi(\tau_2))$, and so on.

The application of this technique can be not only cumbersome and time consuming, but also inaccurate if the injected signal is large. For example, Fig. 6(a) shows how the ISF of a 4-GHz ILO can be determined through simulation by injecting an impulse (in this case a 5-mV, 10-ps pulse) into an oscillator at various phases, ϕ, in relation to the oscillator output. Once this ISF has been determined, it is possible to use the method described by Fig. 5 to predict the ILO's sensitivity to other injected signals. In Fig. 6(b) the amplitude of the applied signal has been increased by a factor of 10. Using the ISF, one would expect the resulting oscillator phase shift to also increase by a factor of 10. Similar predictions can be made for an increase in pulse width, as shown in Fig. 6(c). Simulations of the ILO show that these predictions are relatively accurate, so long as the resulting phase shifts remain smaller than approximately 10 degrees. Unfortunately, larger phase shifts are often required in order to implement an ILO with a wide lock range or a fast lock time. Fig. 6(d) shows a large injected pulse amplitude, such as would be required in a fast-locking ILO. The ISF prediction method in this case greatly overestimates the actual phase shifts.

IV. The Phase Domain Response

In this work, simulations are also used to develop the ILO model; however, instead of simulating the ILO under impulsive injection and feeding the result into complex, and in some cases inaccurate, expressions, we instead simulate the ILO's phase transient with the actual injected pulse shape being studied. As a result, the proposed method can be viewed as an extension of the ISF model, which allows the circuit designer to easily translate simulation results into an understanding of ILO behavior. Due to the speed at which these simulations can be performed, the proposed technique allows for fast iterations of the design process, thereby enabling quick progression towards design goals. Moreover, the resulting model is accurate even under strong injection, and is readily incorporated into behavioral simulations.

To define the model we begin by defining the relationship between the injected signal and the ILO output. First, we assume that when the ILO is locked by some injected signal to an angular frequency ω_{lock}, its output is

$$V_{out}(t) = f\left(\omega_{lock} t + \theta(t)\right) \tag{6}$$

where f is some periodic function with period 2π describing the oscillating waveshape (e.g., square, sinusoidal, etc.) and $\theta(t)$

represents the phase of the signal.[1] Similarly, the injected signal can be represented by

$$V_{inj}(t) = b\left(\frac{\omega_{lock}}{N}t + \theta_{inj}(t)\right) \tag{7}$$

where b is some periodic function (i.e., a sinusoid or a pulse train) with period 2π, $\theta_{inj}(t)$ is the phase of the injected signal and N is an integer that represents some multiplication factor between the injected and ouput signal frequencies. In this paper, the behavior of ILOs under either fundamental or subharmonic injection frequencies (i.e., N $\geq$ 1) are considered. Although there is no reason to believe that these techniques cannot be applied to ILOs under superharmonic injection, the work required to prove this was outside the scope of this paper.

In the case where the injected signal is no longer present, the ILO will free-run at a frequency $\omega_0 = \omega_{lock} - \Delta\omega$, and its output becomes

$$V_{out}(t) = f\left((\omega_{lock} - \Delta\omega)t + \theta(t)\right) \tag{8}$$

where $\theta(t)$ again represents the phase of the ILO output, which may not be equal to the $\theta(t)$ from (6) depending on the injected signal. Here, $\Delta\omega$ is the difference between the frequency of the locked ILO and its free-running frequency,

$$\Delta\omega = \omega_{lock} - \omega_0. \tag{9}$$

In this work, the oscillator's response to one full period of the injected signal, $V_{inj}(t)$, is simulated. If the ILO includes any peripheral circuitry such as narrow pulse generators to condition the injected signal then this can be included in the simulation to ensure that the effects of this circuitry are accurately captured. Each period of this injected signal changes the phase of the ILO's output, $\theta(t)$, by an angle, P. This phase change depends upon $\phi(t)$, defined as the phase of the ILO output signal $\theta(t)$ subtracted from the phase of the injected signal, $\theta_{inj}(t)$, such that

$$\phi(t) = \theta_{inj}(t) - \theta(t). \tag{10}$$

Note that in this work, the phase difference between the injected and output signals is defined simply by the difference in their zero crossings.

Hence, we define the phase domain response (PDR), $P(\phi)$, as the ILO's phase change for each injection of one period of $V_{inj}(t)$ as a function of the relative phase of this injection, $\phi(t)$. The PDR is readily extracted from a series of transient simulations, as demonstrated by Fig. 7 where two samples of $P(\phi)$ are determined by applying one period of $V_{inj}(t)$ at phases ϕ_1 and ϕ_2.

Since the PDR is specific to the injected signal, $V_{inj}(t)$, it can have a wide variety of possible shapes depending on the amplitude, shape and frequency of the injected signal and the injection scheme used. While this technique means that PDR simulations must be redone if the injected pulse shape is changed, these simulations can be run in a short time and the results are accurate and provide insight.

[1]Note that voltage state variables $V(t)$ are used in this work, any of the relevant signals may be branch currents instead of voltages.

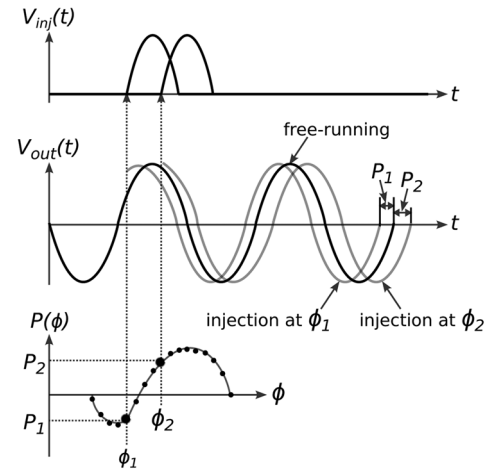

Fig. 7. The PDR, $P(\phi)$, is determined through simulation by applying one period of the injected signal, $V_{inj}(t)$, at different phases, ϕ_n, relative to the oscillator's output signal, V_{out}, and observing the resulting change in output phase, P.

V. PDR-Based ILO Modeling

With the PDR in hand, a behavioral model for the ILO is formed under the assumption that injection of the waveform b at a relative phase ϕ causes an immediate change in the ILO's output phase equal to $P(\phi)$.[2] Moreover, it is assumed that, apart from the phase shifts resulting from these injection events, the ILO continues to operate at its free-running frequency, ω_0, causing its phase relative to the lock frequency to drift by $2\pi\Delta\omega/\omega_0$ radians each period.

If we treat each period of the injected signal as a discrete event then we are interested in the phase difference at the start of the kth injection and (10) becomes

$$\phi_k = \theta_{inj,k} - \theta_k. \tag{11}$$

While an ILO is locking, the difference between the injected signal phase and ILO output phase evolves along the sequence $\phi_1, \phi_2, \ldots \phi_k$. This means that the phase shift introduced by injection event k is $P(\phi_k)$ such that

$$\phi_{k+1} = \phi_k - P(\phi_k). \tag{12}$$

The negative sign is included because an increase in ILO output phase results in future injection events being applied earlier relative to the ILO output.

In the event that $\omega_{lock} \neq \omega_0$ (i.e., $\Delta\omega \neq 0$) an additional phase shift of $-2\pi N\Delta\omega/\omega_0$ is added to (12). The resulting expression for the phase difference between the injected signal and the ILO output becomes

$$\phi_{k+1} = \phi_k - P(\phi_k) - \frac{2\pi N\Delta\omega}{\omega_0} \tag{13}$$

Finally, since any perturbations of the phase of the injected signal phase (i.e., cycle-to-cycle jitter) can be represented as

$$\Delta\theta_{inj,k} = \theta_{inj,k+1} - \theta_{inj,k} \tag{14}$$

[2]This is an approximation since, in fact, it may generally take some time for the ILO's output phase to react to the injected input. However, the accuracy of this approximation is borne out by later comparison of the model with transistor-level simulations and measurements.

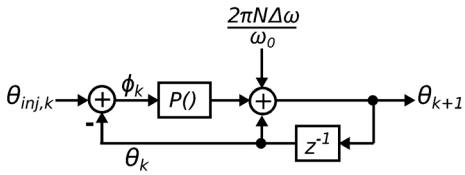

Fig. 8. Model representing the nonlinear phase relationship between the injected signal and the ILO output.

this should be included in the model and (13) becomes

$$\phi_{k+1} = \phi_k - P(\phi_k) - \frac{2\pi N \Delta\omega}{\omega_0} + \Delta\theta_{inj,k} \tag{15}$$

One may also wish to consider the ILO's behavior in terms of an absolute phase reference in order to model external phase perturbations and to make this model applicable in other, larger systems. This can be done by substituting (11) into (15), resulting in

$$\theta_{k+1} = \theta_k + P(\phi_k) + \frac{2\pi N \Delta\omega}{\omega_0} \tag{16}$$

This relationship incorporates the nonlinear PDR, $P(\phi_k)$, and can be represented by the system drawn in Fig. 8. The absolute phase reference of this model means that it can easily be implemented to model ILO behavior in system level simulations.

Equations (16) and (11) and Fig. 8, comprise a general nonlinear behavioral model of an ILO. The nonlinear PDR function, $P()$, may be extracted from a relatively quick series of transient simulations of the ILO to be modeled, as described above. In the next section, it will be shown how $P()$ may also be extracted from measurements of an ILO. The following sections will show how the model may be used to very quickly and accurately find the phase relationship, lock range, lock time and tracking bandwidth of an ILO. Each of these ILO performance metrics would otherwise require extensive transistor-level simulations; hence, the model greatly accelerates design iterations, affording the designer insight. The model may also be integrated into larger behavioral system-level models such as phase-locked loops and clock distribution networks.

A. Steady-State Phase Shift

When locked, the oscillator and injected pulses will settle to some steady-state phase relationship, ϕ_{ss}, where each injected period causes a phase shift $P(\phi_{ss})$ that is just sufficient to cancel the phase drift resulting from $\Delta\omega$. In order for an ILO, with free-running frequency of ω_0 to lock to ω_{lock}, the phase change produced by each period of the injected signal at steady-state, $P(\phi_{ss})$, must be sufficient to eliminate the phase drift accumulated over N cycles of the oscillator output such that

$$P(\phi_{ss}) = -\frac{2\pi N \Delta\omega}{\omega_0}. \tag{17}$$

Equation (17) shows that the steady-state phase relationship, ϕ_{ss}, between the injected signal and the ILO output is determined by the frequency difference, $\Delta\omega$. This observation is intuitive since the steady-state phase relationship between the injected and output signals, ϕ_{ss}, of an ILO has previously been exploited in applications such as clock deskew, where ILO output phase can be adjusted by tuning the free-running frequency of a VCO [3].

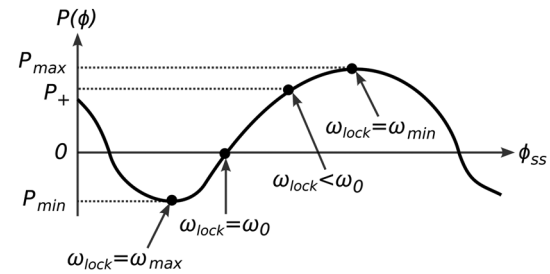

Fig. 9. Steady-state phase relationships are determined by the difference between ω_{lock} and ω_0.

Fig. 9 illustrates this concept by showing the steady-state phase, ϕ_{ss}, relationship between the injected signal and the oscillator output for a variety of injection frequencies. When $\omega_{lock} = \omega_0$ the injected pulses have no need to influence the oscillator's output and therefore settle to a steady-state relationship where, according to the PDR, they will have no effect on the output phase (i.e., $P(\phi) = 0$). When $\omega_{lock} < \omega_0$ each injected pulse must decrease the oscillation frequency, meaning that the pulses settle to a steady-state relationship where they will each create a positive change in oscillator phase, given in this example by P_+. These steady-state relationships are reached, after some settling time, regardless of the phase at which the injected pulses begin.

B. Lock Range

Fig. 9 shows that a natural extension of the steady-state phase shift modeling is that the lock range of an ILO can be determined directly from its PDR since the ILO can only successfully lock to an injected signal that produces a large enough phase change in the oscillator output to compensate for the difference in their frequencies. In other words, the maximum value of $\Delta\omega$, which we define to be $\Delta\omega_{high}$, can be found using (17) to be

$$\Delta\omega_{high} = -\frac{\omega_0 P_{min}}{2\pi N}. \tag{18}$$

Similarly, the minimum value of $\Delta\omega$, which we define to be $\Delta\omega_{low}$, is

$$\Delta\omega_{low} = -\frac{\omega_0 P_{max}}{2\pi N}. \tag{19}$$

The total output referred lock range, $\Delta\omega_{max}$, is therefore

$$\Delta\omega_{max} = \Delta\omega_{high} - \Delta\omega_{low} \tag{20}$$

$$= \frac{\omega_0 (P_{max} - P_{min})}{2\pi N} \tag{21}$$

$$= \frac{\omega_0 P_{pp}}{2\pi N} \tag{22}$$

where $P_{pp} = P_{max} - P_{min}$ has been defined as the peak-to-peak value of the PDR. Simulation results of an example oscillator topology comparing these lock range equations to SPICE-level simulations are presented in Section VI-A.

Treating the maximum and minimum PDR values separately, as in (18) and (19), identifies cases where the lock range is not centered equally about the free-running frequency. This effect

can be present in ILOs for a variety of reasons, especially during strong injection and is often ignored in ILO models. Although it has been reported and incorporated into a model in [9], this work was limited to the specific case of an LC-ILO using an inductor with a low Q factor. In contrast, the lock range calculation given by (22) does not require that the circuit designer determine an effective Q, injection strength, or any other oscillator parameter. Instead it relies only on the PDR, which can be efficiently extracted from simulation of any ILO.

C. Lock Time

When an injected signal is applied, the time that it takes for an ILO's output to settle to some steady-state phase relationship with this injection is known as the lock time. This transient relationship can be useful in determining the ILO's jitter tracking capabilities [11] and can also be important in applications that require fast locking, such as frequency hoping [15], burst mode [16] or fast power-on applications [4].

The PDR allows us to predict lock time variations that are not obvious in the frequency-domain ILO model. Although it has been shown that the frequency domain model can be manipulated to predict these lock time variations [15], the complexity introduced by such manipulations can make this approach unattractive. Whereas it is usually suggested that lock time depends only upon $\Delta\omega$ and injection strength, the PDR model indicates that there is also a strong dependence on the initial phase relationship, ϕ_0, between the ILO output and the injected signal.

For the analysis of lock time, however, we assume that no phase perturbations are introduced by the injected signal ($\Delta\theta_{inj,k} = 0$). In this case, the model given by (15) shows that the ILO phase will settle to its steady-state condition, ϕ_{ss}, when

$$\phi_{k+1} = \phi_k = \phi_{ss} \tag{23}$$

and therefore

$$P(\phi_k) = P(\phi_{ss}) = -\frac{2\pi N \Delta\omega}{\omega_0} \tag{24}$$

which corresponds to (17) as determined previously.

To reach this state, an injected signal that begins at a phase that is far from the desired steady-state relationship, ϕ_{ss}, will require more injection events, and therefore a longer time, to reach ϕ_{ss}. Fig. 10 demonstrates this relationship for an example case where two identical injected signals are applied individually to an ILO at initial phases ϕ_{0_1} and ϕ_{0_2}. Since ϕ_{0_1} is much closer to ϕ_{ss} than ϕ_{0_2}, this means that $\Delta\phi_1 < \Delta\phi_2$, which results in a shorter lock time for the injected signal that begins at ϕ_{0_1}. Note that although $P(\phi_u) = P(\phi_{ss})$, the steady-state ILO output phase cannot settle to this point. A small deviation to the left of ϕ_u, resulting from noise or a slight frequency difference between ω_{lock} and ω_0, will produce a small positive phase shift, which will then shift the phase difference further to the left of ϕ_u, in turn producing a larger positive phase shift, and so on until ϕ_{ss} is reached. A similar effect occurs in the opposite direction if the shift occurs to the right of ϕ_u. Due to the small

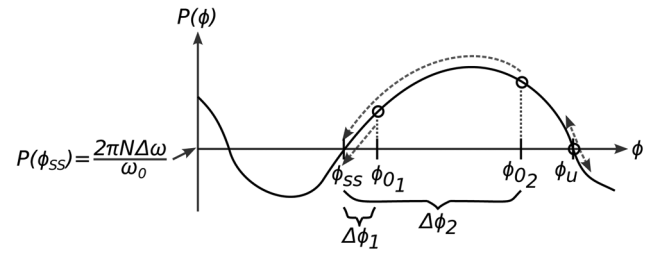

Fig. 10. An ILO's lock time depends on the initial phase difference, $\Delta\phi$, between the injected signal ϕ_0 and the steady-state phase difference, ϕ_{ss}, required by the frequency of the injected signal.

steps that begin this settling, the increase in lock time that occurs when $\phi_0 = \phi_u$ is significant.

To illustrate this effect, Fig. 11(a) shows the PDR of a 4-stage ring oscillator obtained using SPICE simulations of a 400-mV_{pp} (differential) injected pulse with a width of 70 ps. Note that in these simulations the phase difference between the injected and output signals is defined by the difference between their zero crossings. When this injected signal is at a frequency close to ω_0 then ϕ_{ss} is where $P(\phi_{ss}) = 0$ on the rising edge of the PDR, as indicated. If the injected signal begins its injection at a phase that is close to ϕ_{ss} it will therefore settle quickly, following a simple, first order exponential settling step response. Indeed, the time constant of this exponential settling is expressed in the following section as a function of the jitter tracking bandwidth, f_{TB}, in (30), in accordance with other linear modeling approaches. If the injected signal begins farther from ϕ_{ss}, especially if it begins near the unstable operating point ϕ_u, it will require a much longer lock time. This effect is captured by the PDR model as shown in Fig. 11(b) where 2 identical signals are injected into the 4-stage ring oscillator but beginning at initial phases ϕ_{0_1} and ϕ_{0_2}, respectively. This can lead to large variations in the lock time of an ILO for a given injection frequency, but is not captured by traditional analyses based on frequency domain modeling.

A more complete picture of the lock time of an ILO as a function of its initial phase is shown in Fig. 12 for both SPICE simulations and as predicted using the PDR model. In these simulations the lock time is defined as the time taken for the oscillator's output phase to settle to within 1° of its steady-state phase. Although the lock time reaches a maximum value near 12 ns, it should be noted that there is no fundamental limit to this and it is possible to observe very long settling times in an ideal, noise-free simulation environment. In practice noise will push the oscillator phase away from ϕ_u, thereby causing it to lock more quickly.

D. Tracking Bandwidth

Although a strength of the PDR-based model is that it captures the nonlinear phase response of the ILO during large phase transients, it can also be used to find linear performance metrics in the presence of small phase deviations such as phase tracking bandwidth. Specifically, consider an ILO that has reached steady-state at a lock point with a relative phase shift ϕ_{ss} defined by (17). Small phase perturbations around this lock point due to phase changes (i.e., jitter) in the injected signal, $\theta_{inj,k}$, result in restoring phase shifts that are proportional to the

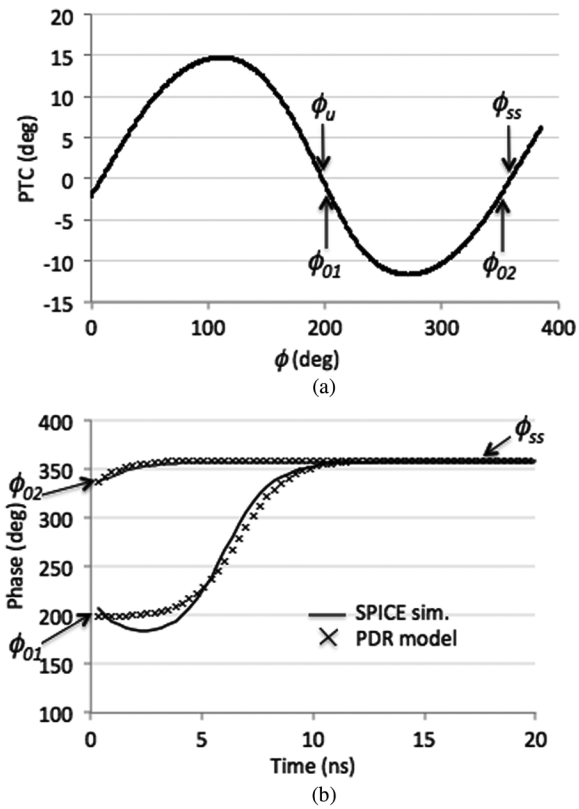

Fig. 11. PDR (a) and transient phase response (b) of a 4-stage ring ILO. When injection begins far from ϕ_{ss} at ϕ_{0_1} the lock time is longer than when it begins at ϕ_{0_2}.

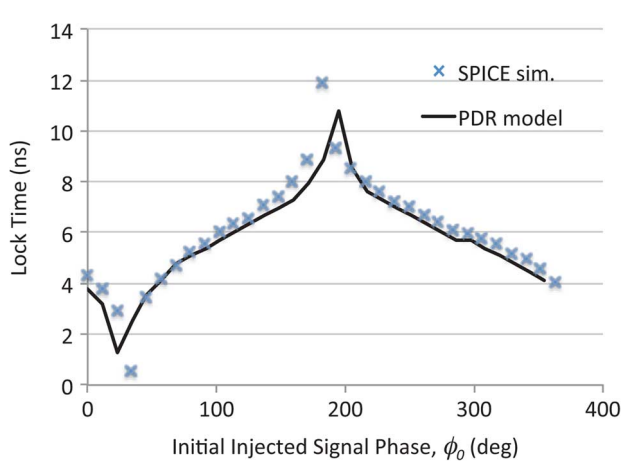

Fig. 12. Lock time varies greatly depending on the phase at which the injected signal begins. This effect is seen in both SPICE-level simulation and the PDR-based lock time model.

phase error. The constant of proportionality is the slope, m, of the PDR around ϕ_{ss}. Hence, under small phase perturbations, a first-order jitter tracking model may be applied,

$$JTF = \frac{1}{1 + \frac{j\,\omega_j}{\omega_{TB}}} \tag{25}$$

where JTF is the jitter tracking function, j is an imaginary number, ω_j is the frequency of the jitter and the 3-dB tracking bandwidth is given by ω_{TB}.

When the phase at the input of the ILO is perturbed by an amount, $\theta_{inj,k}$, then the output phase of the ILO can be determined using (16) as

$$\theta_{k+1} = \theta_k + P(\theta_{inj,k} - \theta_k) - P(\phi_{ss}) \tag{26}$$

This equation shows that the rate of change of the output phase of the ILO in response to $\theta_{inj,k}$ is determined by P. To determine the jitter tracking bandwidth of the system, we apply a small step change to $\theta_{inj,k}$ and observe the system response as illustrated in Fig. 8. When this step is applied, the phase difference between the injected signal and the ILO output, ϕ_k, jumps by the value of the applied step, which then causes the output phase θ_{k+1} to change by $P(\phi_k)$, according to (26).

Since the output phase follows a first order exponential settling, as shown in the previous section, the time constant τ_{TB} of this response can be found from the slope of θ_{k+1}. This can be determined by taking the derivative of (26), resulting in

$$\frac{d\theta_{k+1}}{d\phi_k} = \frac{dP(\phi_k)}{d\phi_k}. \tag{27}$$

If we assume that for small perturbations in θ_{inj} the slope of P is a constant given by m then

$$m = \left.\frac{dP(\phi_k)}{dk}\right|_{\phi_k = \phi_{ss}} \tag{28}$$

and the time constant, τ_{TB}, of the settling behavior can be defined as

$$\tau_{TB} = \frac{1}{m f_{inj}} \tag{29}$$

where f_{inj} is included to convert τ_{TB} from injection cycles to seconds. This then means that the jitter tracking bandwidth of the first-order phase tracking model is given by

$$f_{TB} = \frac{1}{2\pi\tau_{TB}} = \frac{m f_{inj}}{2\pi} \tag{30}$$

where the injected frequency, f_{inj}, is related to Δf and therefore ϕ_{ss} through (17).

To verify the accuracy of this model, the f_{TB} of the 4-stage ring oscillator discussed in the previous section is calculated using the PDR shown in Fig. 11 in conjunction with (28)to (30). The result is compared to SPICE simulations of small phase perturbations over a range of injected frequencies in Fig. 13.

VI. Wide Lock Range ILO Design

This section presents a design example applying the proposed model to a multiplying ILO (MILO) that generates a 4-GHz output signal from a 1-GHz reference clock. In order to demonstrate the usefulness of the PDR model, the MILO is designed to have a very wide lock range, which is difficult to model using other methods. Wide lock range is typically difficult to achieve for ILOs, with reported lock ranges commonly less than 5% of the free-running frequency [1], [4]. Hence, an unconventional circuit architecture is required that doesn't fit conventional ILO

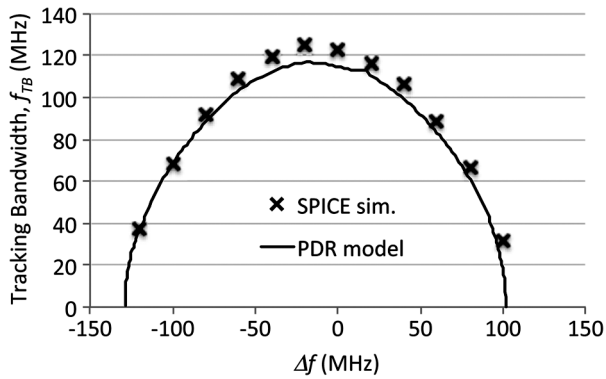

Fig. 13. The 3-dB jitter tracking bandwidth can be accurately predicted over a range of injected frequencies using the PDR model.

models, but the PDR-based model can be applied easily and is shown to accurately predict performance.

A ring oscillator topology was chosen for this work. The frequency domain model presented in [3] states that the lock range of a ring oscillator-based ILO is

$$\Delta\omega_{max} = \frac{2\omega_0}{n \sin\frac{2\pi}{n}} \frac{K}{1-K^2} \tag{31}$$

where n is the number of stages in the ring and K is the relative injection strength given as I_{inj}/I_{osc}. Although this model indicates that the number of oscillator stages should be decreased and that the injection strength should be increased in order to maximize $\Delta\omega_{max}$, the model provides very little insight into what the injected signal should look like and how it should be applied to the MILO. Further complicating the application of the frequency domain model is the fact that (31) must be modified once the loosely defined boundary between weak and strong injection is crossed.

The PDR model, specifically (22), indicates that the lock range, Δf_{max}, can be increased by maximizing the peak-to-peak phase domain response, P_{pp}. Since P_{pp} can be efficiently determined through simulation, the lock range of different MILO topologies can be quickly evaluated and compared. In this design a lock range of 1 GHz, or 25% of the 4-GHz f_0 was targeted, which translates to a target P_{pp} of 360°.

To serve as a starting point in the design, a four-stage CML ring oscillator was simulated in a standard 65-nm GP CMOS process. To create a strong injected signal strength, V_{inj} was applied to a secondary input differential pair with the drain nodes connected to those of the original CML stage as shown in Fig. 14. The tail current of the injection pair was chosen to be 1/5 of the main oscillator differential pair in order to ensure that the ILO continues to oscillate when there is no injected signal present. Varactor load capacitances are used to tune the MILO's free-running frequency if necessary.

The PDR of the four-stage MILO is then determined by simulation using injected pulses with an amplitude of 300 mV_{pp} (differential) and a width equal to approximately half of one period of a 4-GHz clock signal. These pulses were applied to the first stage of the oscillator, as shown in Fig. 15. In order to create a realistic pulse shape in the simulation environment, an ideal pulse is first applied to a CML differential pair before it is applied to the MILO. The secondary differential pair shown in

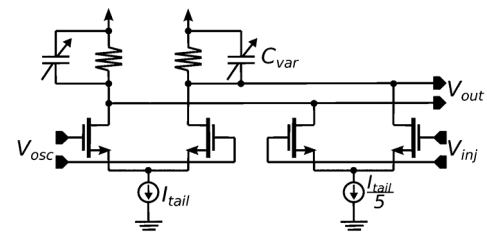

Fig. 14. One stage of the four-stage CML injection locked ring oscillator. Applying the injected signal to a secondary differential pair provides a strong injection strength.

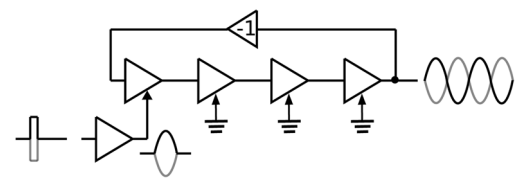

Fig. 15. The PDR is determined by measuring the output phase change created when a single pulse is applied to the MILO at different phases relative to the oscillator's output signal.

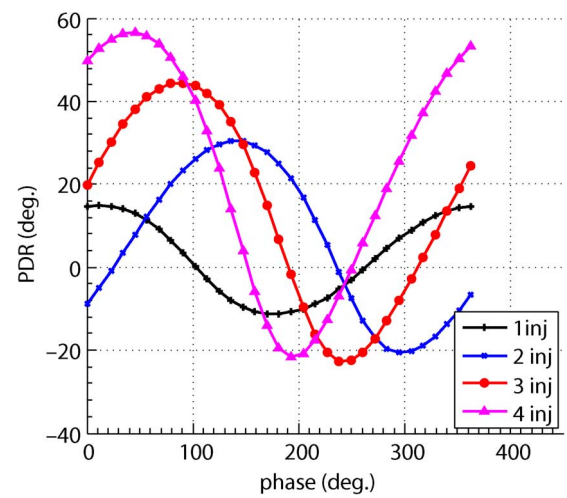

Fig. 16. Simulation results show that the peak-to-peak amplitude of the PDR increases as more injection sites are added.

Fig. 14 is included in each stage of the oscillator to provide a consistent load at the output of each stage. Where these injection pairs are unused, their gates have been grounded.

By applying this pulse at various times spanning one period of the clock signal and observing the resulting change in the output phase of the MILO, the PDR was determined and is plotted as the "1 inj" curve in Fig. 16. It exhibits a P_{pp} of 26°, which corresponds to a lock range of 54 MHz and highlights the difficulty of achieving a wide lock range for an ILO. Although the strength of the injected signal has been maximized relative to the available headroom in the 65-nm CMOS process, other strategies that attempt to increase the MILO's sensitivity to injected signals are required in order to increase lock range.

A. Injection Point Selection

Injection into multiple locations of an oscillator has been shown to increase the lock range of injection-locked frequency dividers by applying the injected signal to the tail currents of two [10] or three different stages of an n-stage ring oscillator [17]. In both cases off-chip controls were used to modify the phase relationship between the injected signals, demonstrating

TABLE I
COMPARISON OF LOCK RANGES CALCULATED USING THE ISF MODEL [6] AND THE PDR MODEL TO THOSE OBTAINED DIRECTLY USING EXTENSIVE SPICE-LEVEL SIMULATIONS

	# inj. sites	1	2	3	4
ISF theory [6]	Δf_{low}	101 MHz	249 MHz	466 MHz	475 MHz
	Δf_{high}	87 MHz	174 MHz	226 MHz	242 MHz
PDR model (this work)	P_{max}	14.7^0	30.4^0	44.4^0	56.5^0
	P_{min}	-11.6^0	-20.61^0	-22.69^0	-21.64^0
	Δf_{low}	32 MHz	67 MHz	97 MHz	124 MHz
	Δf_{high}	25 MHz	45 MHz	50 MHz	47 MHz
Spectre sim.*	Δf_{low}	30 MHz	60 MHz	90 MHz	120 MHz
	Δf_{high}	30 MHz	40 MHz	50 MHz	50 MHz

*performed with 10 MHz resolution

that injected signals should be applied with successive phase delays of π/n in order to achieve the widest lock range. In other words, the injected signal should experience the same delay as is created by one oscillator stage before being injected into the subsequent stage. This means that the required phase shift in the injected signal can be easily created on-chip by passing the injecting signal through delay elements that are identical to those that make up the ring oscillator [4].

The addition of each new injection site increases the ILO's sensitivity to an injected pulse. This is illustrated in Fig. 16 where the peak-to-peak value of the PDR is increased as the number of injection sites increases from injection into a single stage ("1 inj") to injection into all four ring oscillator stages ("4 inj"). Although the effects of this multi-stage injection would be difficult to predict using conventional ILO models, the PDR is readily determined through simulation and the results can easily be translated into the resulting lock range, lock time, or tracking bandwidth, as discussed in the previous sections.

It should be noted that the limited bandwidth of each element in the delay line used to duplicate the delays of the ring oscillator stages results in the loss of some high frequency content of the injected pulse as it travels through each successive stage. This means that the pulse, which began with a width equal to half the bit period of the output clock will become wider by the time it reaches the final stage of the ring. These wide pulses are therefore able to produce a larger positive phase change in the MILO output, which corresponds to improved locking to frequencies lower than that of the free-running oscillator. They are, however, not able to improve locking to higher frequencies, resulting in a lock range that is not symmetric about the oscillator's free-running frequency. Although this effect is typically not addressed by existing ILO models, it is clearly visible in the difference between positive and negative peak values in Fig. 16.

The peak PDR values were translated to lock ranges using (22) and are reported in Table I. These results are compared to lock ranges obtained using the ISF method [6] and to those obtained directly from SPICE-level simulation using Virtuoso Spectre. To obtain the lock range in this way the transient response of the oscillator was simulated over a range of frequencies and a locked condition is identified by the settling of the MILO's output phase (relative to a reference signal) to some steady-state value. In order to ensure that the MILO is locked and that there is no eventual slipping in the output phase, the transient simulation must be run for several hundred clock cycles. This, combined with the fact that the step size of the frequency sweep must be small in order to accurately determine the lock range, results in simulations that consume a significant amount of time and resources. This highlights the usefulness of determining this information using the PDR method instead.

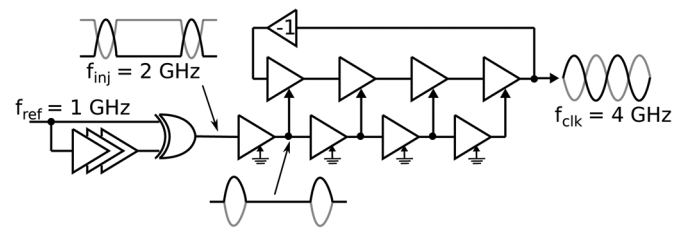

Fig. 17. Creating pulses at the reference clock edges emphasizes the desirable harmonic of the input thereby improving the lock range of the MILO.

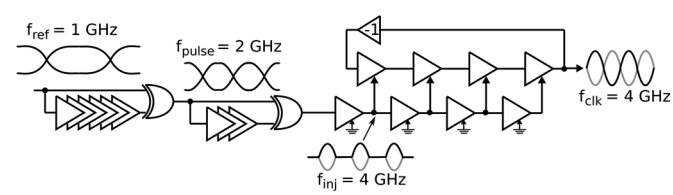

Fig. 18. The addition of a second edge detector with wide pulse widths further emphasizes the desired harmonic of the input signal.

B. Frequency Pre-Conditioning

Another method of increasing the lock range of a multiplying ILO is to introduce a frequency pre-conditioning circuit that emphasizes the input's desirable harmonic. For example, an edge detector comprising a delay and XOR gate, as shown in Fig. 17 is often used for this purpose [4], [16].

While the impact of adding an edge detector to the MILO would be difficult to include in existing ILO models, its inclusion in the PDR simulations is trivial. First, the delays and XORs shown in Fig. 17 were included prior to the ILO. Then a dc offset was added to the first amplification stage in the delay chain in order to create the return-to-zero pulses shown in this figure. Simulations of the MILO using this injection technique show that it increases Γ_{pp} to 114°. Further increases are then achieved by adding a second edge detector set to create pulse widths equal to twice that of the original edge detector, resulting the MILO topology shown in Fig. 18. Using this technique increases Γ_{pp} to 204°.

Furthermore, with the injected pulses now arriving at almost the same frequency as the output clock, it becomes unnecessary for the injected signal to return to zero between injected pulses and a full swing sinusoid can now be used as the injection signal instead. Note that this circuit was reported in [18] as a technique for implementing a frequency-multiplier with wide op-

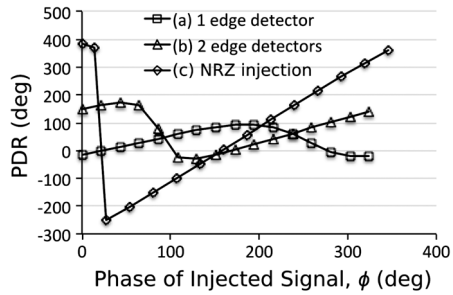

Fig. 19. PDR curves for ILOs using (a) one edge detector, (b) two edge detectors and (c) two edge detectors used to produce a sinusoidal (NRZ) injection signal.

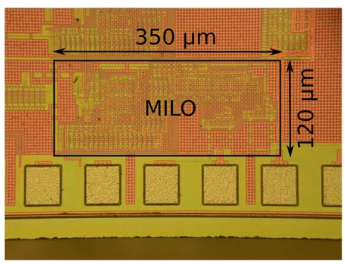

Fig. 20. Die photo of the MILO fabricated in 65-nm GP CMOS.

erating range and fast power-on functionality but no model for the ILO was presented. Simulations of this circuit show that Γ_{pp} increases beyond the target value of 360°. The simulated PDR curves for the case of one edge detector, two edge detectors, and two edge detectors without return-to-zero (NRZ) injection, are shown in Fig. 19. The PDR values reported for the case of two edge detectors with sinusoidal injection indicate that a 4-GHz ILO using this topology should be able to achieve a lock range that extends 0.7 GHz above f_0 [using (18)] and 1.06 GHz below f_0 [using (19)].

VII. Measured Results

To validate the predictions of the PDR model, the MILO, including both edge detectors, was fabricated in a 65-nm GP CMOS process. A die photo of this prototype, which consumes 0.042 mm^2, is shown in Fig. 20.

Direct measurement of the PDR of an ILO is impractical since it can be exceedingly difficult to apply of a single period of the injected signal and to observe the real-time change in the output phase. Instead it is possible to obtain part of the PDR indirectly using the relationship described by (17). Since the fabricated ILO was designed to have a multiplication factor of $N = 4$ and was measured to have an $\omega_0 = 4$ GHz, it is possible to measure the resulting values of ϕ_{ss} as various frequency offsets, $\Delta\omega$, are applied. In order to ensure that there are no changes in the phase of the injected signal introduced by the test setup, frequency offsets are applied by keeping ω_{inj} constant and varying the ω_0 of the ILO, which is accomplished in this design by varying varactor voltages. Fig. 21(a) compares the ϕ_{ss} values measured in this way to those obtained from SPICE-level simulations. Fig. 21(b) then translates these measurements to the PDR using (17) and compares them to the PDR that is obtained through simulation as discussed in the previous sections.

The measured lock range of the fabricated device is from 3 GHz to 4.7 GHz, or 42.5% of the 4-GHz free-running frequency.

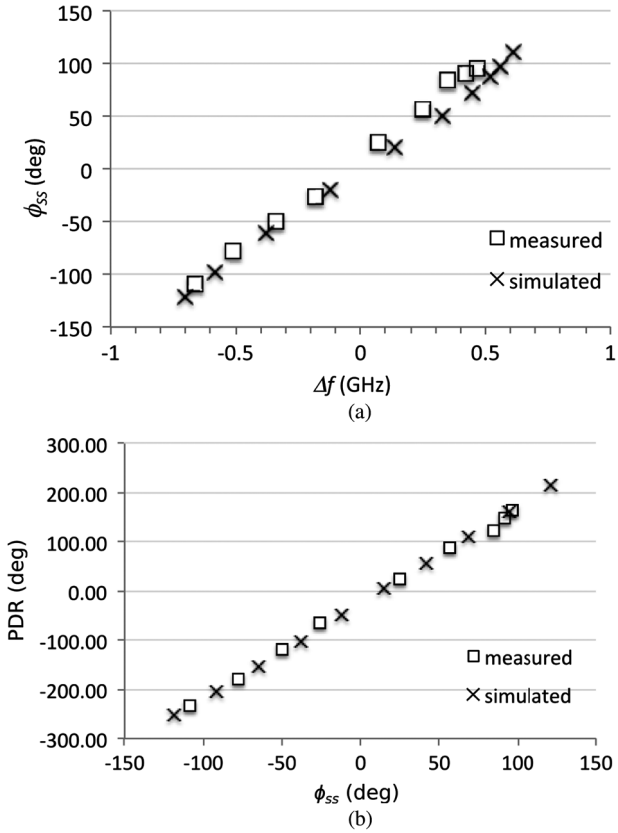

Fig. 21. Measured values of (a) ϕ_{ss} for various frequency offsets can be translated to (b) the PDR of the ILO. These measurements show good agreement with SPICE-level simulations.

TABLE II
Comparison of Measured Lock Ranges to Those Calculated Using the PDR Model

PDR model (this work)	P_{max}	383.3^0
	P_{min}	-250.9^0
	Δf_{low}	1.06 GHz
	Δf_{high}	0.7 GHz
Measured	Δf_{low}	1 GHz
	Δf_{high}	0.7 GHz

This compares well with the lock range that was predicted by the PDR, as can be seen in the comparison shown in Table II. The PDR model predicts not only the total lock range accurately but also the asymmetry of this lock range.

VIII. Conclusion

Modeling ILO behavior by using conventional frequency domain models requires the use of several parameters which are difficult to define. Modeling using the ISF-based model is accurate and applicable only when the injected signal strength is low. As an alternative, the proposed PDR model of an oscillator can be used in conjunction with simple transistor-level simulations to accurately predict the behavior of any ILO under any injected signal. This makes the PDR model useful during the design of an ILO, helping to optimize the circuit for a given set of requirements.

Using this PDR model a MILO was designed to multiply a 1-GHz reference clock by 4 to produce a 4-GHz output clock. By simulating the PDR of the MILO at various stages

throughout the design process, it was possible to quickly evaluate the impact that each change in topology had on the lock range. This in turn made it possible to achieve the target lock range in a logical progression of design steps, resulting in a MILO with a measured lock range equal to 42.5% of the free-running frequency.

REFERENCES

[1] I.-T. Lee and S.-I. Liu, "G-band injection-locked frequency dividers using π-type LC networks," *IEEE Trans. Circuits Syst. I, Reg. Papers*, vol. 59, no. 2, pp. 315–323, Feb. 2012.

[2] L. Liu, T. Sakurai, and M. Takamiya, "315 MHz energy-efficient injection-locked OOK transmitter and 8.4 μW power-gated receiver front-end for wireless Ad Hoc network in 40 nm CMOS," in *Proc. IEEE Symp. VLSI Circuits*, Jun. 2011, pp. 278–279.

[3] M. Hossain and A. Chan Carusone, "CMOS oscillators for clock distribution and injection-locked deskew," *IEEE J. Solid-State Circuits*, vol. 44, no. 8, pp. 2138–2153, Aug. 2009.

[4] J. Zerbe, B. Daly, and W. Dettloff *et al.*, "A 5.6 Gb/s 2.4 mW/Gb/s bidirectional link with 8 ns power-on," in *Proc. IEEE Symp. VLSI Circuits*, Jun. 2011, pp. 82–83.

[5] R. Adler, "A study of locking phenomena in oscillators," *Proc. IRE*, vol. 34, no. 6, pp. 351–357, 1946.

[6] P. Maffezzoni, "Analysis of oscillator injection locking through phase-domain impulse-response," *IEEE Trans. Circuits Syst. I, Reg. Papers*, vol. 55, no. 5, pp. 1297–1305, Jun. 2008.

[7] A. Hajimiri and T. Lee, "A general theory of phase noise in electrical oscillators," *IEEE J. Solid-State Circuits*, vol. 33, no. 2, pp. 179–194, Feb. 1998.

[8] L. Paciorek, "Injection locking of oscillators," *Proc. IEEE*, vol. 53, no. 11, pp. 1723–1727, Nov. 1965.

[9] M. Mansuri, F. O'Mahony, and G. Balamurugan *et al.*, "Strong injection locking of low-Q LC oscillators," in *Proc. IEEE Custom Integr. Circuits Conf.*, Sep. 2008, pp. 699–702.

[10] A. Mirzaei, M. Heidari, and R. Bagheri *et al.*, "Injection-locked frequency dividers based on ring oscillators with optimum injection for wide lock range," in *Proc. IEEE Symp. VLSI Circuits*, Sep. 2006, pp. 174–175.

[11] M. Hossain and A. Chan Carusone, "5-10 Gb/s 70 mW burst mode AC coupled receiver in 90-nm CMOS," *IEEE J. Solid-State Circuits*, vol. 45, no. 3, pp. 524–537, Mar. 2010.

[12] A. Mirzaei, M. Heidari, and A. Abidi, "Analysis of oscillators locked by large injection signals: Generalized adler's equation and geometrical interpretation," in *Proc. IEEE Custom Integr. Circuits Conf.*, Sep. 2006, pp. 737–740.

[13] D. Leeson, "A simple model of feedback oscillator noise spectrum," *Proc. IEEE*, vol. 54, no. 2, pp. 329–330, Feb. 1966.

[14] X. Lai and J. Roychowdhury, "Capturing oscillator injection locking via nonlinear phase-domain macromodels," *IEEE Trans. Microw. Theory Tech.*, vol. 52, no. 9, pp. 2251–2261, Sep. 2004.

[15] N. Lanka, S. Patnaik, and R. Harjani, "Understanding the transient behavior of injection locked LC oscillators," in *Proc. IEEE Custom Integr. Circuits Conf.*, Sep. 2007, pp. 667–670.

[16] J. Lee and M. Liu, "A 20-Gb/s burst-mode clock and data recovery circuit using injection-locking technique," *IEEE J. Solid-State Circuits*, vol. 43, no. 3, pp. 619–630, Mar. 2008.

[17] J.-C. Chien and L.-H. Lu, "Analysis and design of wideband injection-locekd ring oscillators with multiple-input injection," *IEEE J. Solid-State Circuits*, vol. 42, no. 9, pp. 1906–1915, Sep. 2007.

[18] D. Dunwell and A. Chan Carusone, "A 2.3–4 GHz injection-locked clock multiplier with 55.7% lock range and 10-ns power-on," in *Proc. IEEE Custom Integr. Circuits Conf.*, Sep. 2012.

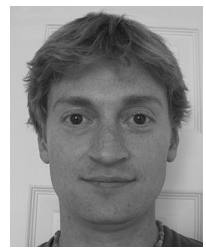

Dustin Dunwell received the Ph.D. degree from the University of Toronto, ON, Canada, in 2012 and the B.Sc. and M.Sc. degrees in from Queen's University, Kingston, ON, Canada in 2004 and 2006 respectively. His M.Sc. and Ph.D. research has been supported by NSERC grants and has focused on high speed integrated circuit design in CMOS technologies. It has ranged from the modeling and optimization of passive devices, to the design of broadband transceiver circuit blocks suitable for multi-gigabit per second transmission over lossy channels. He is currently working for Kapik Integration, Toronto.

Anthony Chan Carusone (SM'08) received his Ph.D. degree from the University of Toronto, ON, Canada, in 2002. Since 2001 he has been with the Department of Electrical and Computer Engineering at the University of Toronto where he is currently a Professor and the Associate Chair, Research. In 2008 he was a visiting researcher at the University of Pavia, Italy, and later at the Circuits Research Lab of Intel Corp., Hillsboro, OR, USA. He is also an occasional consultant to industry in the areas of integrated circuit design, clocking, and digital communication.

Prof. Carusone was a co-author of the best student papers at the 2007, 2008, and 2011 Custom Integrated Circuits Conferences, the best invited paper at the 2010 Custom Integrated Circuits Conference, and the best paper at the 2005 Compound Semiconductor Integrated Circuits Symposium. He is also an author, along with David Johns and Ken Martin, of the 2nd edition of the classic textbook *Analog Integrated Circuit Design*. He is an appointed member of the Administrative Committee of the IEEE Solid-State Circuits Society and the Circuits and Systems Society's Board of Governors. He has served on the technical program committee for the Custom Integrated Circuits Conference, and is currently a member of the technical program committees for the VLSI Circuits Symposium and International Solid-State Circuits Conference. He has been a guest editor for the IEEE TRANSACTIONS ON CIRCUITS AND SYSTEMS—PART I: REGULAR PAPERS and was on the editorial board of the IEEE TRANSACTIONS ON CIRCUITS AND SYSTEMS—PART II: EXPRESS BRIEFS from 2006 until 2009 when he was Editor-in-Chief. He is currently an Associate Editor of the IEEE JOURNAL OF SOLID-STATE CIRCUITS.